World Academy of Science, Engineering and Technology
International Journal of Aerospace and Mechanical Engineering
Vol:18, No:7, 2024

Non-reacting Numerical Simulation of Axisymmetric Trapped Vortex Combustor

Heval Serhat Uluk, Sam M. Dakka, Kuldeep Singh, Richard Jefferson-Loveday

***Abstract*—**This paper will focus on the suitability of a trapped vortex combustor as a candidate for gas turbine combustor objectives to minimize pressure drop across the combustor and investigate aerodynamic performance. Non-reacting simulation of axisymmetric cavity trapped vortex combustors was run to investigate the pressure drop for various cavity aspect ratios of 0.3, 0.6 and 1 and for air mass flow rates of 14 m/s, 28 m/s and 42 m/s. A numerical study of an axisymmetric trapped vortex combustor was carried out by using two-dimensional and three-dimensional computational domains. A comparison study was conducted between Reynolds Averaged Navier Stokes (RANS) k-ε Realizable with enhanced wall treatment and RANS k-ω Shear Stress Transport (SST) models to find the most suitable turbulence model. It was found that the k-ω SST model gives relatively close results to experimental outcomes. The numerical results were validated and showed good agreement with the experimental data. Pressure drop rises with increasing air mass flow rate, and the lowest pressure drop was observed at 0.6 cavity aspect ratio for all air mass flow rates tested, which agrees with the experimental outcome. A mixing enhancement study showed that 30-degree angle air injectors provide improved fuel-air mixing.

***Keywords*—**Aerodynamic, Computational Fluid Dynamics, Propulsion, Trapped Vortex Combustor.

NOMENCLATURE

d_{aft}	Afterbody Diameter
d_c	Combustor Diameter
d_{ca}	Diameter of the Cavity Air Injector
d_f	Forebody Diameter
d_{fuel}	Fuel Injection Diameter
d_s	Spindle Diameter
g	Acceleration due to gravity
k	Turbulent Kinetic Energy (J)
L	Length of the Combustor
L_{air1}	Distance of Inner Cavity Air Injection
L_{air2}	Distance of Outer Cavity Air Injection
L_{ca}	Cavity Length
L_f	Distance of Fuel Injection
NO_x	Nitrogen Emission
P_r	Prandtl Number
S	Modulus of the mean-rate of strain tensor
t_{aft}	Thickness of Afterbody
t_f	Thickness of Forebody

Greek

G_b	Turbulence kinetic energy from buoyancy
G_k	Kinetic energy from mean velocity gradient
σ_{ij}	Stress tensor that generated by molecular viscosity
S_k, S_ε	Source Terms
μ_t	Turbulence viscosity
ν_T	Eddy viscosity
Y_M	Addition of fluctuating dilation in compressible turbulence to overall dissipation

Abbreviation

PISO	Pressure-Implicit with Splitting of Operators
PRESTO	Pressure Staggering Option
QUICK	Quadratic Upstream Interpolation for Convective Kinematics
RANS	Reynolds Averages Navier-Stokes
SST	Shear-Stress Transport
TVC	Trapped Vortex Combustor

I. INTRODUCTION

TRAPPED VORTEX COMBUSTOR concept is an alternative combustor design that could increase the combustion characteristics, and it can be used for alternative fuels. It was first introduced in [1], and it is considered to be good replacement for conventional swirl stabilized gas turbine combustor. Gas turbine combustors use a swirl-stabilizer to create continuous source of ignition for incoming fuel which reduces flame stability and combustion efficiency significantly [2], [3]. However, trapped vortex combustor relies on vortex that created in cavity to produce sustainable flame. Fuel and air directly injected to inside this cavity, which gives control over equivalence ratio at primary zone of combustion process. Moreover, these cold fuel and air injected inside cavity act as cooling agent for combustion zone the prevent over-heating as well as it improves the mixing of air and fuel [4].

Main advantages of the first generation trapped vortex combustors are [1], [4]-[7]:

- Extremely low pressure drops across the combustor.
- Low NO_x emission
- Low Lean-blow-out limit
- High combustion efficiency
- Operating under various inlet velocities and equivalence ratios.

Trapped vortex combustor idea is stems from the drag reduction studies of bluff bodies [8], [9]. In these works, it was found that minimum drag can be achieved around cavity aspect ratio of $0.6d_f$ (forebody diameter). The same result was also observed in [1]. Their experiment showed that lowest pressure drop observed exactly at certain cavity aspect ratio under cold flow conditions. Moreover, in their result it is stated that even under combustion conditions this value is only subjected a small change, with $0.6d_f$. Therefore, it can be concluded that in order to design combustor dimensions cold flow experiment is

Heval Serhat Uluk is with University of Nottingham, UK (e-mail: heval.uluk@nottingham.ac.uk).

a good measure of deciding a configuration which has the lowest pressure drop.

Computational fluid dynamics has an important role nowadays to estimate fluid behaviors, which reduces cost of an experiment subsequently. Because the combustor configurations can be tested first with the numerical simulations to estimate optimum dimensions with lowest pressure drop and drag. After deciding most suitable configuration via numerical simulations, experiments can be conducted by manufacturing a combustor that meets all the combustor criteria. Therefore, it is important to have turbulence model that can estimate the cold flow behavior for trapped vortex combustor. This paper will investigate the most suitable turbulence model for axisymmetric trapped vortex combustor. It will also investigate effect of air injectors angle on fuel air mixing.

II. Problem Description

Axisymmetric trapped vortex combustor is used with two-dimensional computational domain to reduce the computation time, but it was necessary to use three-dimensional domain for mixing enhancement study because of the injections inside cavity.

The axisymmetric configuration was adopted from [1]. The cavity is between two bluff bodies, which are called forebody and afterbody, and propane used as a fuel for this configuration (Fig. 1). Two bluff bodies are connected via with a spindle (9 mm), which is used for carrying air and fuel to afterbody where air and fuel injectors located. 24 air injection points are placed surrounding the 8 fuel injectors (Fig. 2). Cavity length (L_{ca}) is an important parameter, and it is adjustable by moving afterbody along the spindle. The forebody has 70 mm (d_f) diameter and afterbody has 50.8 mm diameter, which are surrounded by an 80 mm diameter and 150 mm long Pyrex tube, and the blockage ratio at the inlet is 76% [1]. The cavity air and fuel injectors turned off for non-reacting experiments to measure pressure drop across combustor, therefore injectors turned off for the simulations as well. Three different annular velocity (14, 28, and 42 m/s) and the cavity length were changed to observe their impact on vortex aerodynamics. In Fig. 5 cavity length normalized with forebody diameter is shown to demonstrate pressure loss percentage.

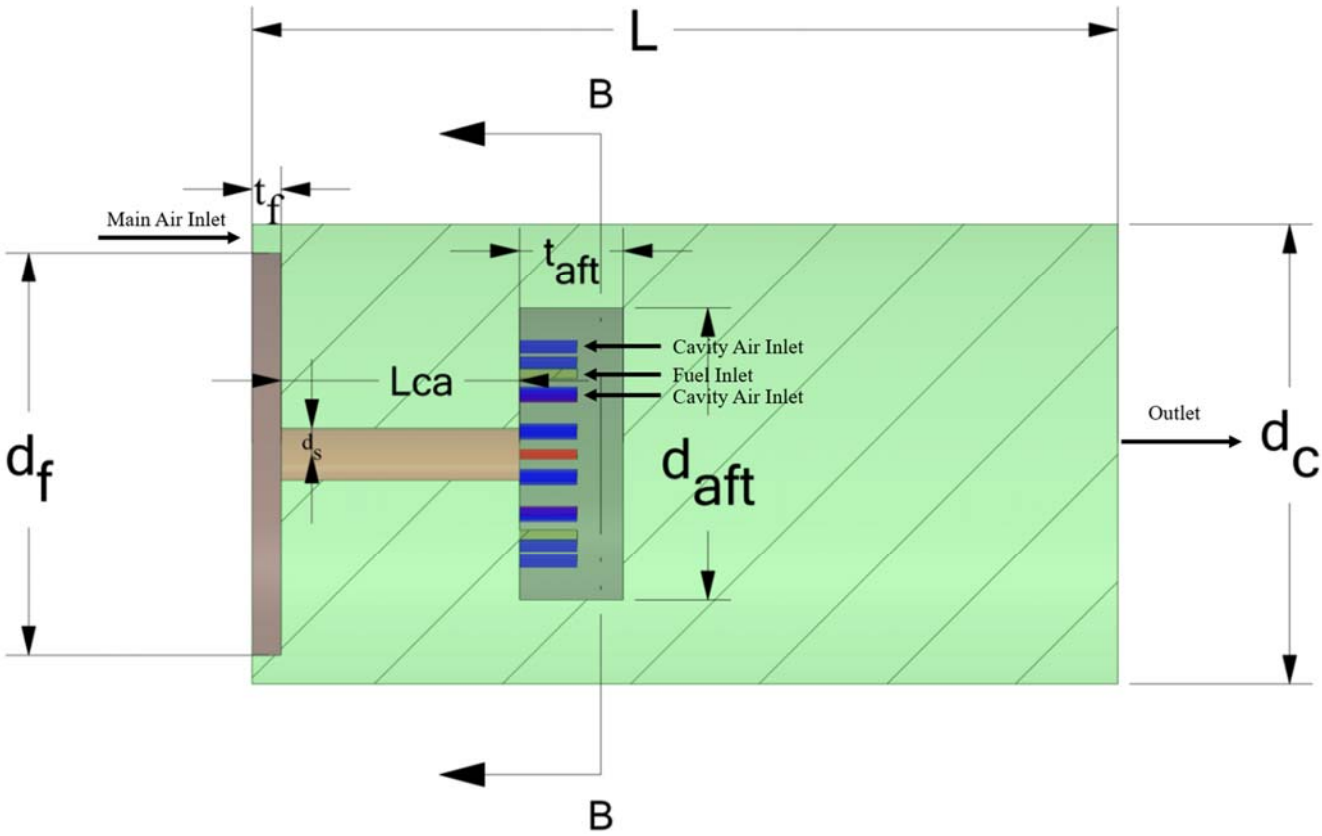

Fig. 1 Side-view of Axisymmetric Trapped Vortex Combustor adopted from [1]

III. Numerical Methodology

A. Governing Equations

In this study, RANS k-ε realizable and RANS k-ω SST (Shear Stress Transport) models are used. The equations to solve RANS k-ε realizable are [10]:

Continuity Equation:

$$\frac{\delta \rho}{\delta t} + \frac{\delta}{\delta x_i}(\rho \bar{u}_i) = 0 \quad (1)$$

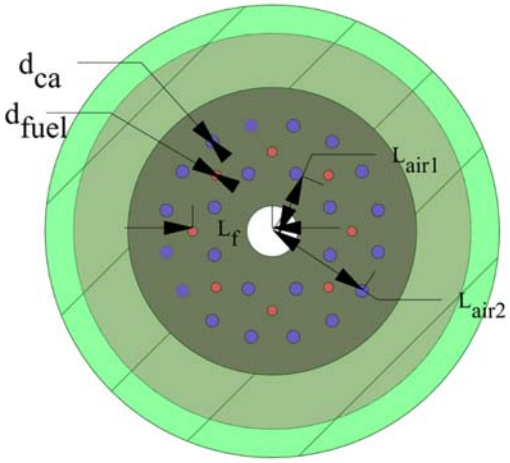

Fig. 2 Cavity Injection Points of Axisymmetric Trapped Vortex Combustor adopted from [1]

TABLE I
GEOMETRY DIMENSIONS FOR AXISYMMETRIC TRAPPED VORTEX COMBUSTOR

Abbreviation	Description	Dimension
L (mm)	Combustor Length	150
d_f (mm)	Forebody Diameter	70
d_c (mm)	Combustor Diameter	80
d_{aft} (mm)	Afterbody Diameter	50.8
d_s (mm)	Spindle Diameter	9
L_{ca} (mm)	Cavity Length	41.3
d_{fuel} (mm)	Fuel Injection Diameter	1.75
d_{ca} (mm)	Cavity Air Injection Diameter	2.29
L_{air1} (mm)	Distance of Inner Cavity Air Injection	11
L_{air2} (mm)	Distance of Outer Cavity Air Injection	19
L_f (mm)	Distance of Fuel Injection	14
t_{aft} (mm)	Thickness of Afterbody	18
t_f (mm)	Thickness of Forebody	5

Momentum Equation:

$$\frac{\delta}{\delta t}(\rho\bar{u}_i) + \frac{\delta}{\delta x_j}(\rho\bar{u}_i\bar{u}_j) = \frac{\delta}{\delta x_j}(\sigma_{ij}) - \frac{\delta\bar{p}}{dx_i} - \frac{\delta\tau_{ij}}{\delta x_j} \quad (2)$$

σ_{ij} refer to stress tensor that generated by molecular viscosity,

$$\sigma_{ij} = \left[\mu\left(\frac{\delta\bar{u}_i}{\delta x_j} + \frac{\delta\bar{u}_j}{\delta x_i}\right)\right] - \frac{2}{3}\mu\frac{\delta\bar{u}_l}{\delta x_l}\delta_{ij} \quad (3)$$

and $\delta\tau_{ij}$ is the subgrid-scale stress, which is described as,

$$\tau_{ij} \equiv \rho\overline{u_i u_j} - \rho\bar{u}_i\bar{u}_j \quad (4)$$

Transport equation of k is defined as:

$$\frac{\delta}{\delta t}(\rho k) + \frac{\delta}{\delta x_j}(\rho k u_j) = \frac{\delta}{\delta x_j}\left[(\mu + \frac{\mu_t}{\sigma_k})\frac{\delta_k}{\delta x_j}\right] + G_k + G_b - \rho\varepsilon - Y_M + S_k \quad (5)$$

G_k is turbulence kinetic energy from mean velocity gradient, whereas G_b is turbulence kinetic energy from buoyancy. Y_M is the addition of fluctuating dilation in compressible turbulence to overall dissipation.

$$G_k = \mu_t S^2 \quad (6)$$

$$S = \sqrt{2S_{ij}S_{ij}} \quad (7)$$

$$S_{ij} = \frac{1}{2}\left(\frac{\delta u_j}{\delta x_i} + \frac{\delta u_i}{\delta x_j}\right) \quad (8)$$

$$G_b = -g\frac{\mu_t}{i\rho Pr_t}\frac{\delta p}{\delta x_i} \quad (9)$$

μ_t is the turbulence viscosity, S is the modulus of the mean-rate of strain tensor, Pr_t turbulent Prandtl number and g is the gravity while transport equation of ε can be expressed as:

$$\frac{\delta}{\delta t}(\rho\varepsilon)\frac{\delta}{\delta x_j}(\rho\varepsilon u_j) = \frac{\delta}{\delta x_j}\left[(\mu + \frac{\mu_t}{\sigma_\varepsilon})\frac{\delta_\varepsilon}{\delta x_j}\right] + \rho C_1 S\varepsilon - \rho C_2\frac{\varepsilon^2}{k+\sqrt{\nu\varepsilon}} + C_{1\varepsilon}\frac{\varepsilon}{k}C_{3\varepsilon}G_b + S_\varepsilon \quad (10)$$

σ_k and σ_ε are Prandtl numbers for k and ε while S_k and S_ε are user defined source terms. C_1 is calculated with (11) and (12):

$$C_1 = max\left[0.43, \frac{\eta}{\eta+5}\right] \quad (11)$$

$$\eta = S\frac{k}{\varepsilon} \quad (12)$$

Other model constants defined:

$$C_1 = 1.44\,, C_2 = 1.9\,, \sigma_k = 1\,, \sigma_\varepsilon = 1.2$$

Turbulent Viscosity (μ_t) can be obtained with (13)-(17):

$$\mu_t = qC_\mu\frac{k^2}{\varepsilon} \quad (13)$$

$$C_\mu = \frac{1}{A_0 + A_S\frac{kU^*}{\varepsilon}} \quad (14)$$

$$U^* = \sqrt{S_{ij}S_{ij} + \tilde{\Omega}_{ij}\tilde{\Omega}_{ij}} \quad (15)$$

$$\tilde{\Omega}_{ij} = \Omega_{ij} - 2\varepsilon_{ijk}\omega_k \quad (16)$$

$$\Omega_{ij} = \bar{\Omega}_{ij} - \varepsilon_{ijk}\omega_k \quad (17)$$

$\bar{\Omega}_{ij}$ is the mean rate of rotation tensor, where A_0 = 4.04 and A_S is calculated as:

$$A_S = \sqrt{6}\sin\varphi \quad (18)$$

$$\varphi = \frac{1}{3}\cos^{-1}(\sqrt{6W}) \quad (19)$$

$$W = \frac{S_{ij}S_{jk}S_{ki}}{\tilde{S}^3} \quad (20)$$

Continuity and governing equations are similar for k-ω SST model, but transport models and closure of uncertain terms are

different from k-ε Realizable. Equations (21)-(27) are used to solve k- ω SST model.

Turbulence kinetic energy (k) equation is:

$$\frac{\delta k}{\delta t} + U_j \frac{\delta k}{\delta x_j} = P_k - \beta^* k\omega + \frac{\delta}{\delta x_j}\left[(\nu + \sigma_k \nu_T)\frac{\delta k}{\delta x_j}\right] \quad (21)$$

$$\frac{\delta \omega}{\delta t} + U_j \frac{\delta \omega}{\delta x_j} = \alpha S^2 - \beta \omega^2 + \frac{\delta}{\delta x_j}\left[(\nu + \sigma_\omega \nu_T)\frac{\delta \omega}{\delta x_j}\right] + 2(1 - F_1)\sigma_{\omega 2}\frac{1}{\omega}\frac{\delta k}{\delta x_i}\frac{\delta \omega}{\delta x_i} \quad (22)$$

Eddy viscosity calculated as:

$$\nu_T = \frac{a_1 k}{\max(a_1 \omega, SF_2)} \quad (23)$$

Equations (24)-(27) are used to closure of uncertain terms of (21)-(23):

$$F_2 = \tanh\left[\left[\max\left(\frac{2\sqrt{k}}{\beta^* \omega y}, \frac{500\nu}{y^2 \omega}\right)\right]^2\right] \quad (24)$$

$$P_k = \min\left(\tau_{ij}\frac{\delta U_i}{\delta x_j}, 10\beta^* \omega\right) \quad (25)$$

$$F_1 = \tanh\left[\left[\min\left\{\max\left(\frac{\sqrt{k}}{\beta^* \omega y}, \frac{500\nu}{y^2 \omega}\right), \frac{4\sigma_{\omega 2} k}{CD_{k\omega} y^2}\right\}\right]^4\right] \quad (26)$$

$$CD_{k\omega} = \max\left(2\rho\sigma_{\omega 2}\frac{1}{\omega}\frac{\delta k}{\delta x_i}\frac{\delta \omega}{\delta x_i}, 10^{-10}\right) \quad (27)$$

and the model constants are $\alpha_1 = {}^5/_9$, $\alpha_2 = 0.44$, $\beta_1 = {}^3/_{40}$, $\beta_2 = 0.0828$, $\beta^* = {}^9/_{100}$, $\sigma_{k1} = 0.85$, $\sigma_{k2} = 1$, $\sigma_{\omega 1} = 0.5$, and $\sigma_{\omega 2} = 0.856$.

B. Boundary Conditions

Air is injected both at the front of the domain and the directly inside the cavity whereas fuel is only injected into cavity, and outlet is located at the rear of the TVC (Fig. 1). Main air inlet, cavity air inlet, and fuel inlet was set to velocity inlet, and outlet was defined as pressure outlet. Walls are set as adiabatic and no-slip condition. Table II represents the all the cases that are considered in this paper.

TABLE II
BOUNDARY CONDITIONS FOR AXISYMMETRIC TRAPPED VORTEX COMBUSTOR

Case	Main Air Velocity (m/s)	Cavity Aspect Ratio	Turbulence Model
Case 1	14	0.3	k-ε Realizable with enhanced wall function Model
Case 2	28	0.3	k-ε Realizable with enhanced wall function Model
Case 3	42	0.3	k-ε Realizable with enhanced wall function Model
Case 4	14	0.3	k-ω SST Model
Case 5	28	0.3	k-ω SST Model
Case 6	42	0.3	k-ω SST Model
Case 7	14	0.4	k-ω SST Model
Case 8	28	0.4	k-ω SST Model
Case 9	42	0.4	k-ω SST Model
Case 10	14	0.6	k-ε Realizable with enhanced wall function Model
Case 11	28	0.6	k-ε Realizable with enhanced wall function Model
Case 12	42	0.6	k-ε Realizable with enhanced wall function Model
Case 13	14	0.6	k-ω SST Model
Case 14	28	0.6	k-ω SST Model
Case 15	42	0.6	k-ω SST Model
Case 16	14	1	k-ε Realizable with enhanced wall function Model
Case 17	28	1	k-ε Realizable with enhanced wall function Model
Case 18	42	1	k-ε Realizable with enhanced wall function Model
Case 19	14	1	k-ω SST Model
Case 20	28	1	k-ω SST Model
Case 21	42	1	k-ω SST Model

C. Solution Procedure

In the present study, k-ω SST turbulence model is selected as a baseline turbulence model because it can predict the reversed flow conditions better [11]. Due to the unsteady nature of the vortices generated in TVC, transient simulations are considered in the present work. Coupled scheme is used for pressure-velocity coupling whereas momentum and pressure are solved with second order upwind scheme, and all the residuals are solved till reaching 10^{-6}.

In order to make a comparison study between turbulence models, additional simulations were run for k-epsilon Realizable model with enhanced wall treatment. PISO algorithm was used for pressure-velocity coupling. Quadratic Upstream Interpolation for Convective Kinematics (QUICK) scheme was implemented for Turbulence Kinetic Energy, Turbulence Dissipation Rate, Momentum. Pressure will be solved with Pressure Staggering Option (PRESTO) Scheme.

D. Grid Independent Study

A typical mesh used for two-dimensional axis-symmetric computational domain is shown in Fig. 3. Structured mesh generated in ICEM-CFD, a pre-processor tool of ANSYS has

been used in this study. Grids were systematically refined near the wall so that it can capture the sharp gradients. A typical cell spacing in wall normal direction is kept 0.003 mm and averaged cell spacing in the domain is kept below 0.2 mm. Three meshes with overall cell count, 100,000 (Mesh Number 1), 170,000 (Mesh Number 2) and 325,000 (Mesh Number 3) were investigated (Table III). The cell count in these meshes were systematically increased such that the refined mesh has at least 1.5 times cells in the critical areas as compared to the previous mesh on the recommendation of [12]. The pressure drop is one of the critical parameters which is considered to obtain a grid independent solution. The variation of pressure drops in the radial direction from bottom of the cavity to top of the cavity at an axial position of 9 mm is presented in Fig. 4. It can be observed that numerical predictions of these meshes overlaps with each other.

TABLE III
GRID INDEPENDENCY STUDY FOR AXISYMMETRIC TVC

Case	Mesh Number	Error (%)
Mesh Number 1	100000	1.6059
Mesh Number 2	170000	2.2139
Mesh Number 3	325000	2.1869

Total pressure drop across cavity was observed higher at the bottom of the cavity for Mesh Number 1, but it settled once we increased mesh number and there was no difference between Mesh Number 3 and 4 (Fig. 4). Since the error between these two-mesh numbers was only 0.027%, it was decided to use Mesh Number 2 for Axisymmetric configuration.

IV. Result and Discussion

A. Comparison of Turbulence Models of Axisymmetric Trapped Vortex Configuration

The suitability of two turbulence models viz. k-ω SST and k-ε Realizable is investigated for various aspect ratios and mainstream air velocities. The results obtained from the numerical investigation are presented in Fig. 5 along with the experimental results of [1]. It can be observed that the numerical simulations are sensitive enough to capture the pressure drop trends of the experimental study for all the investigated parameters. In the experimental study pressure drop first decreases with the increase in cavity aspect ratio from 0.3 to 0.6 and thereafter increases as cavity aspect ratio increases to 0.9. This trend is identical for the investigated mainstream air velocities of 14 m/s, 28 m/s and 42 m/s. It can be noticed from Fig. 5 that both turbulence models could capture this trend and predicting optimal cavity aspect ratio accurately.

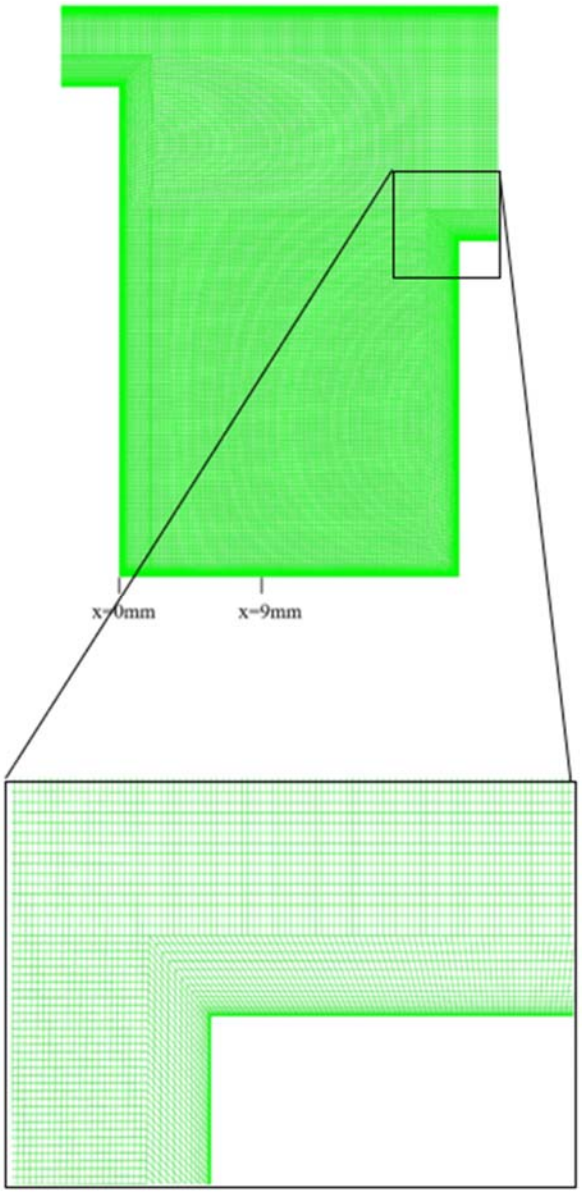

Fig. 3 A typical mesh used for axisymmetric trapped vortex combustor and zoomed view near the wall

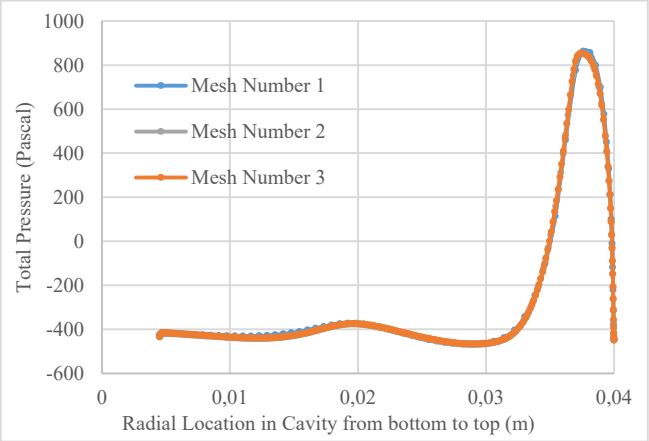

Fig. 4 Grid Independent Study for Total Pressure Drop at x = 9 mm

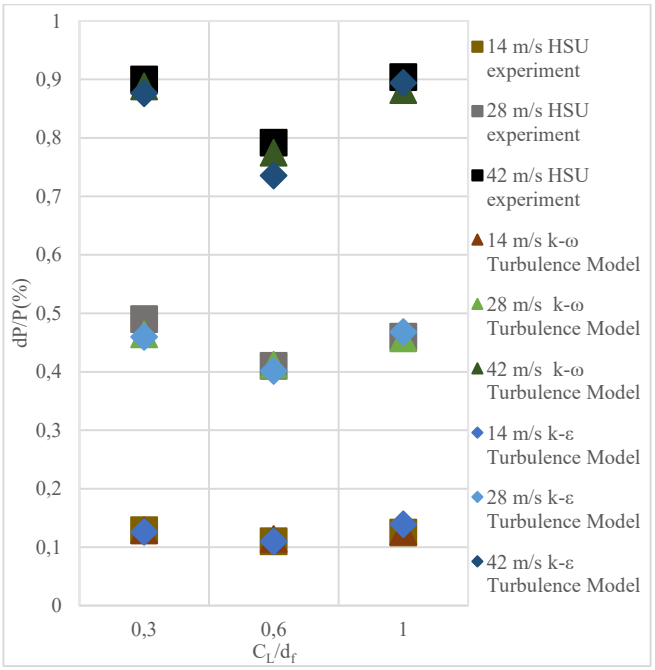

Fig. 5 Compression Study of k-ω SST and k-ε Realizable turbulence models by total pressure drop percentage for 0.3, 0.6 and 1 cavity aspect ratios for 14 m/s, 28 m/s, and 42 m/s main air inlet velocities

It can also be observed that the employed turbulence models can predict different mainstream flow conditions. The total pressure drop inside the combustor is investigated for three mainstream flow conditions i.e., 14 m/s, 28 m/s and 42 m/s. The total pressure drops inside combustor measured lowest around 0.11% for 14 m/s main air inlet velocity at 0.6 cavity aspect ratio. When main air inlet increased from14 m/s to 28 m/s, the pressure drop is almost quadruple, but the lowest pressure drops were still observed at 0.6 cavity aspect ratio with 0.41%. Increasing main air inlet velocity further to 42 m/s made total pressure drop reach to around 0.9%. Even though this increase has increased pressure drop substantially, the lowest total pressure was again at 0.6 cavity aspect ratio. It also should be noted that increasing main air inlet velocity enhanced the difference between maximum and lowest pressure drop among cavity aspect ratios. These trends are well captured by the employed turbulence models.

Moreover, the quantified results indicate that the predictions of k-ω SST turbulence model are close to the experimental results as compared to the k-ε Realizable. For instance, at 42 m/s air inlet velocity and 0.6 cavity aspect ratio, the deviation in the predictions of these turbulence models is noticeable i.e. 7.13%. Therefore, it will be advisable to use, k-ω SST turbulence model for all inlet velocity for two-dimensional simulation domain. However, k-ε Realizable turbulence model is also able to produce correct result with minor error. Since three-dimensional domain will have more mesh number to solve, it is recommended to implement this turbulence model to three-dimensional domain to reduce computational cost.

B. Mixing Enhancement of Fuel and Air

One of the main objectives of TVC is to enhance mixing of air and fuel. Impact of air and fuel injector inclination is not well studied and hence it was decided to extend numerical study to investigate this. The influence of air injectors angle on the mixing performance is studied by varying air injection angle from transverse injection (labeled as 0 degree), and three different angles, 15-degree, 30-degrees, and 45-degrees as shown in Fig. 6. The numerical study was carried out for a cavity air velocity of 10 m/s, with 42 m/s main air velocity and 22 m/s fuel velocity.

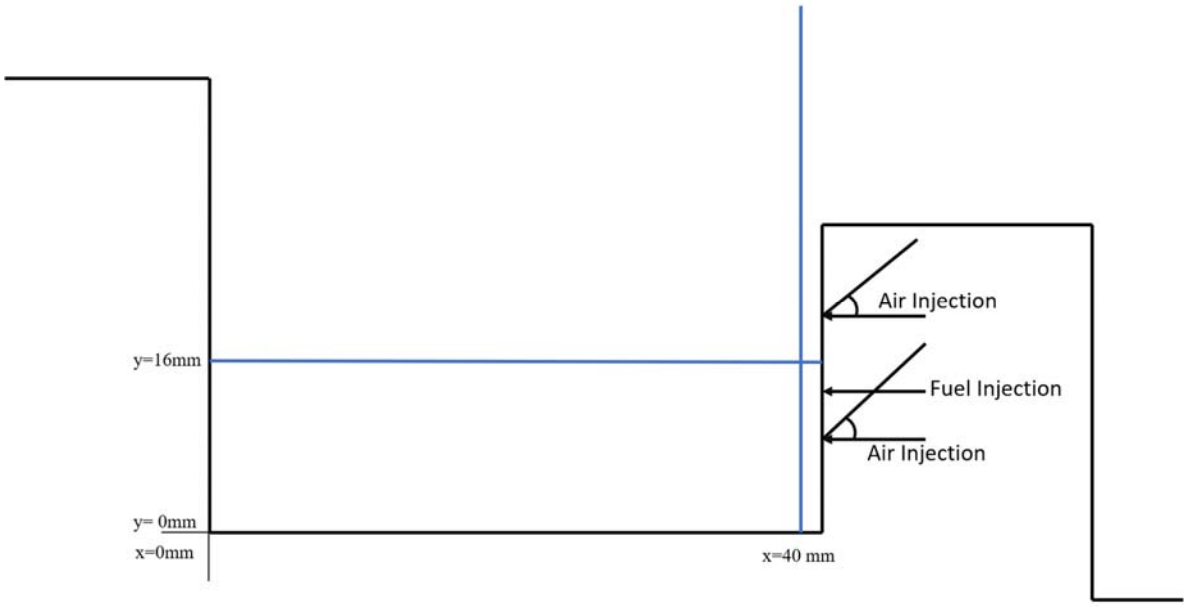

Fig. 6 Axisymmetric Cavity Measurement Locations

It was found that the fuel concentration was the highest at the x = 40 mm, near the fuel injectors, for 0-degree air injectors. Fig. 7 suggest that fuel concentration was in favor to 30-degree air injectors because presence of the high fuel concentration after x = 20 mm indicates that fuel can diffuse throughout cavity. Moreover, fuel concentration at bottom of the cavity was found lower for 30 degree and 45-degree air injection because at these angles air reaches bottom of the cavity near the afterbody, and the fuel is not trapped at the corner of the cavity (see Figs. 9 and 10). This is the reason why fuel concentration is also high for 30-degree air injections. Other significant observation was that fuel concentration around fuel injectors was lower for 30 degree and 45-degree air injector, which is another proof that fuel does not diffuse around fuel injectors and incoming air that comes directly above fuel pushes the fuel inside cavity for oblique injector configuration.

It is also noted that fuel is not only rich on radial direction, the proportion of the fuel was also higher at the axial direction of the cavity for 30 degrees. Especially at the fuel injector location x = 40 mm, fuel concentration was highest for 30-degree air injectors domain, which makes it possible to inject more fuel into main vortex that is shown in Fig. 9. This proves that this configuration can transport fuel to the end of the cavity (Fig. 8).

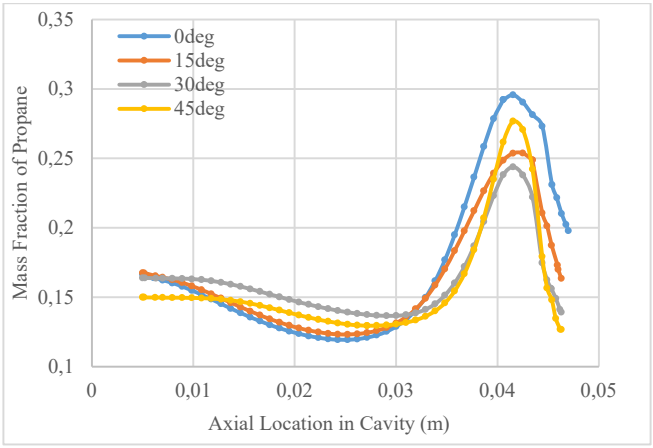

Fig. 7 Mass Fraction of the Propane inside Cavity at y = 16 mm

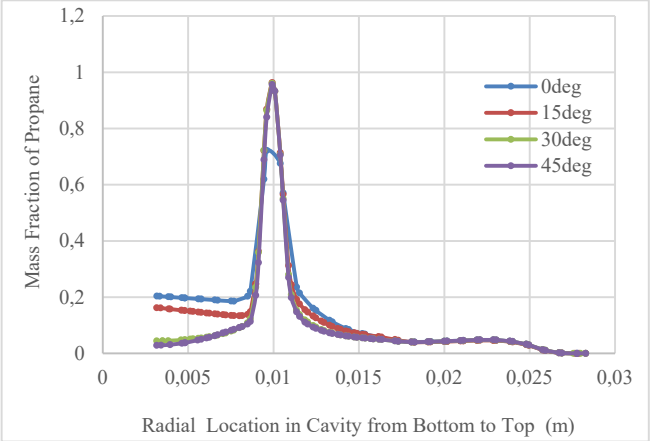

Fig. 8 Mass Fraction of the Propane inside Cavity at x = 40 mm

There was no change observed related to center of the cavity vortex, but altering air fuel injection has effect on fluid at the bottom cavity (Figs. 9 and 10). This aerodynamic change is the basic factor that changes the fuel air mixing inside the cavity by increasing fuel mass fraction after x = 20 mm.

V. Conclusions

In this paper, the suitability of the k-ε Realizable and k-ω SST model for trapped vortex combustor applications was evaluated. It was found that both k-ω SST turbulence model and k-ε Realizable with enhanced wall function model generate favorable results compared with experiment. When it comes to mixing enhancement study it is found that 30 degree diverted air injectors promise high fuel air mixing inside cavity because the fuel concentration was found higher at front of the cavity.

Effect of cavity aspect ratio, main air velocity, and cavity air velocity on trapped vortex combustor was also investigated, and the outcomes are as follows:

- Total pressure drop increases as the cavity aspect ratio increases, with an exception at $0.6d_f$
- The lowest total pressure drop is observed at $0.6d_f$ for axisymmetric TVC for 14 m/s, 28 m/s and 42 m/s
- Total pressure drop rises as the main air inlet velocity increases
- Air injector inclination has a significant impact on the mixing air-fuel characteristics. An injection angle of 30 degree is found to give better mixing.

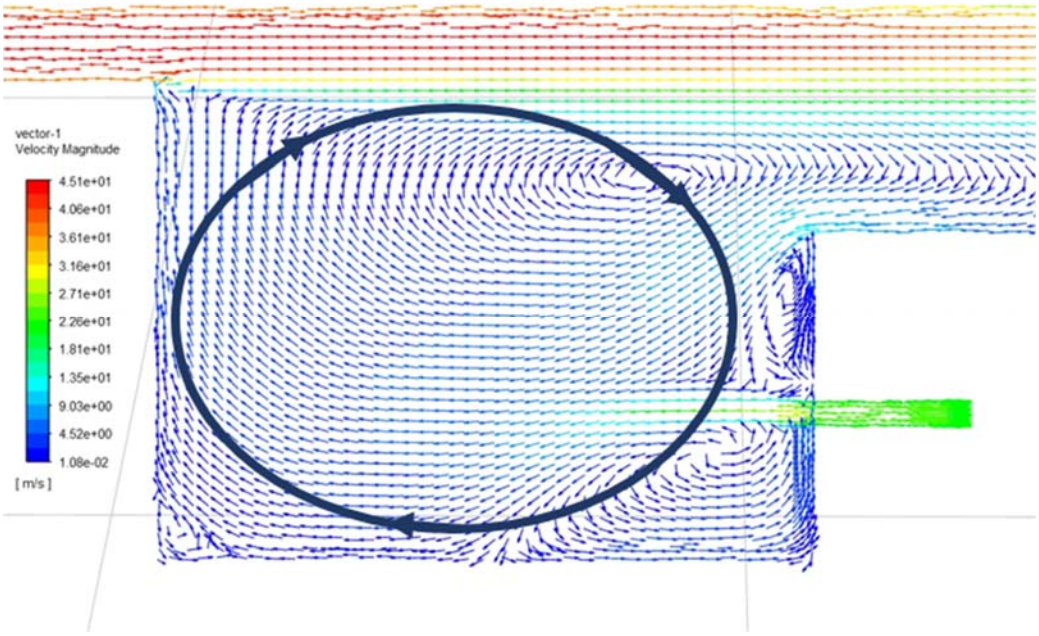

(i)

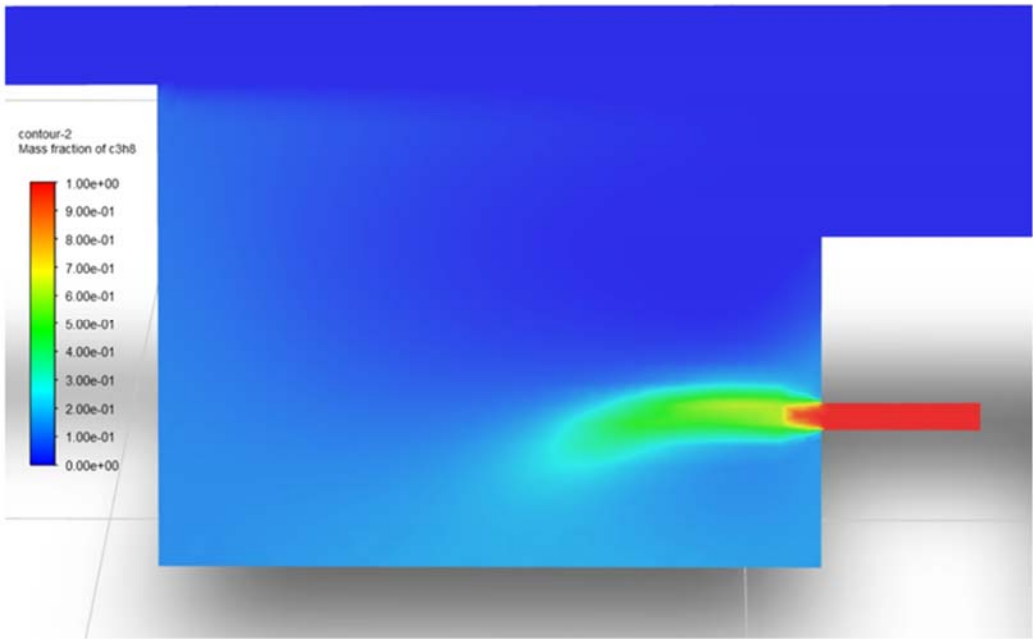

(ii)

Fig. 9 Velocity Vectors (i) and Propane Mass Fraction (ii) at fuel inlet for 0-degree

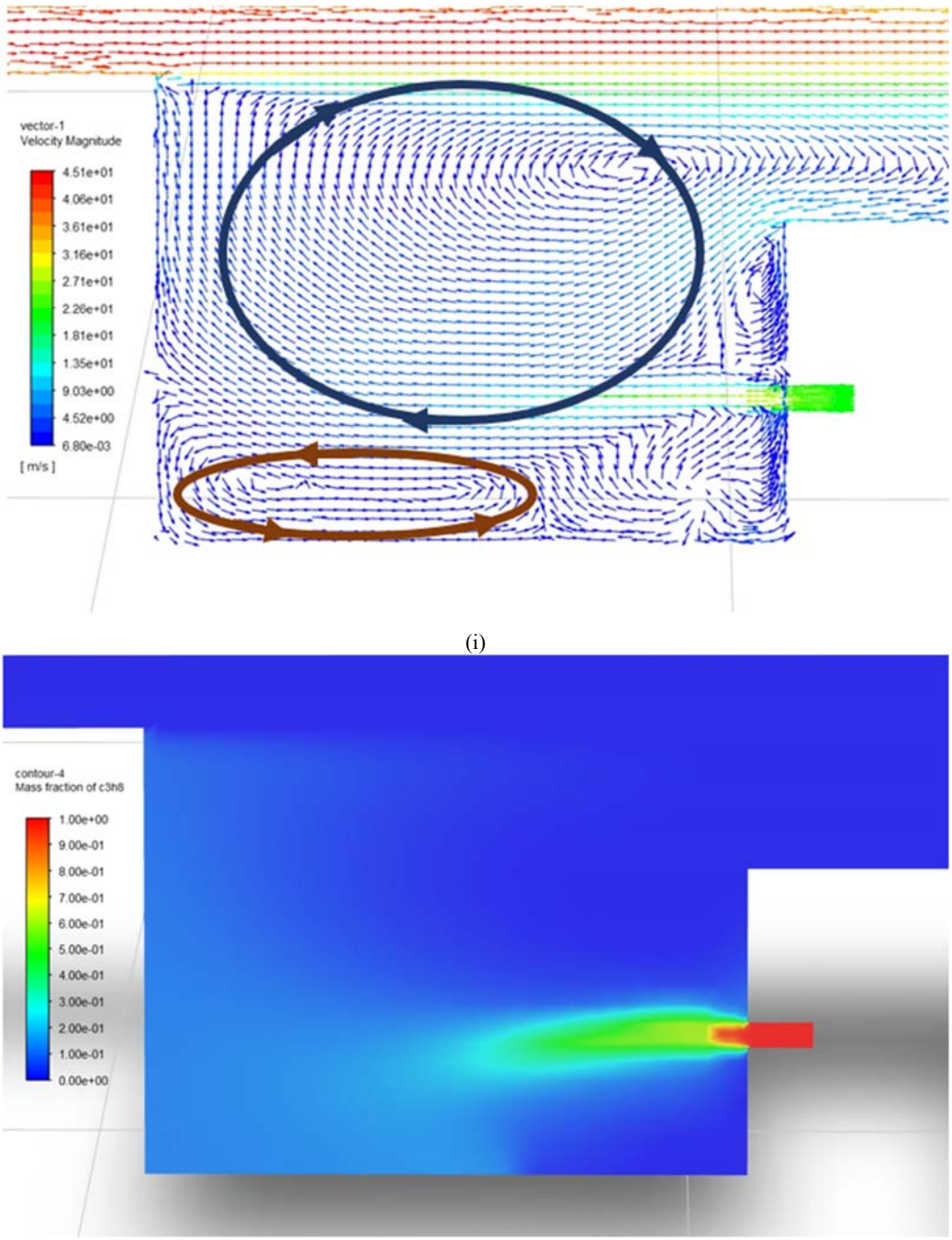

Fig. 10 Velocity Vectors (i) and Propane Mass Fraction (ii) at fuel inlet for 30 degrees

ACKNOWLEDGMENT

Heval Serhat Uluk would like to thank to his supervisors Dr. Sam Dakka and Kuldeep Singh. The author gratefully acknowledges the scholarship from The Republic of Turkey Ministry of National Education for their funding and support.

REFERENCES

[1] K.-Y. Hsu, L. P. Goss, D. D. Trump, and W. M. Roquemore, "Performance of a Trapped-Vortex Combustor."
[2] A. H. Lefebvre and D. R. Ballal, "GAS Turbine Combustion Third Edition Alternative Fuels and Emissions."
[3] P. K. Ezhil Kumar and D. P. Mishra, "Combustion noise characteristics of an experimental 2D trapped vortex combustor," *Aerosp Sci Technol*, vol. 43, pp. 388–394, Jun. 2015, doi: 10.1016/j.ast.2015.03.014.
[4] K. Y. Hsu, L. P. Goss, and W. M. Roquemore, "Characteristics of a trapped-vortex combustor," *J Propuls Power*, vol. 14, no. 1, pp. 57–65, 1998, doi: 10.2514/2.5266.
[5] C. Ghenai, K. Zbeeb, and I. Janajreh, "Combustion of alternative fuels in vortex trapped combustor," *Energy Convers Manag*, vol. 65, pp. 819–828, Jan. 2013, doi: 10.1016/j.enconman.2012.03.012.
[6] A. Singhal and R. V Ravikrishna, "Single cavity trapped vortex combustor dynamics-Part-1: Experiments."
[7] R. C. Hendricks *et al.*, "Experimental and Computational Study of Trapped Vortex Combustor Sector Rig with High-Speed Diffuser Flow," 2001.

[8] W. A. Mair, "The Effect of a Rear-Mounted Disc on the Drag of a Blunt-Based Body of Revolution," *Aeronautical Quarterly*, vol. 16, no. 4, pp. 350–360, Nov. 1965, doi: 10.1017/s0001925900003589.
[9] B. H. Little and R. R. Whipkey, "Locked Vortex Afterbodies," *J Aircr*, vol. 16, no. 5, pp. 289–295, 1979, doi: 10.2514/3.58522.
[10] "Ansys Fluent Theory Guide," 2022. Online. Available: http://www.ansys.com
[11] P. K. Ezhil Kumar and D. P. Mishra, "Numerical simulation of cavity flow structure in an axisymmetric trapped vortex combustor," *Aerosp Sci Technol*, vol. 21, no. 1, pp. 16–23, Sep. 2012, doi: 10.1016/j.ast.2011.04.007.
[12] I. B. Celik and J. Li, "Assessment of numerical uncertainty for the calculations of turbulent tow over a backward-facing step," *International Journal for Numerical Methods in Fluids Int. J. Numer. Meth. Fluids*, vol. 49, pp. 1015–1031, 2005, doi: 10.1002//d.1040.